Multi-carrier Tb/s silicon photonic coherent receiver

Zhen WANG, Xingfeng LI, Jingchi LI, Jian SHEN, Yong ZHANG & Yikai SU*

*State Key Lab of Advanced Optical Communication Systems and Networks, Department of Electronic Engineering,
Shanghai Jiao Tong University, Shanghai 200240, China*

Abstract   We propose a silicon polarization-diversity coherent receiver for wavelength-multiplexing transmission without using the large-footprint arrayed waveguide grating (AWG). We have integrated our proposed coherent receiver on the silicon-on-insulator (SOI) platform for high-capacity transmission. In the proposed coherent receiver, high-frequency photocurrent signals from other wavelengths are suppressed by electrical low-pass filters. Moreover, the signal-signal beat interference (SSBI) generated from each wavelength is eliminated by the balanced detection. These two features lend to the proposed coherent receiver being free of the mm-scale AWG. We have demonstrated our proposed coherent receiver to detect a 1.12-Tb/s wavelength-division-multiplexed and polarization-division-multiplexed 16-ary quadrature amplitude modulation (PDM-16-QAM) signal. The compact footprint of the silicon chip promises small-form-factor receivers for future ultra-high-capacity coherent communication systems that require a high integration level and low fabrication cost.

Keywords   silicon photonics, optical receivers, coherent communication, wavelength-division-multiplexing (WDM), polarization-division-multiplexing (PDM)

1   Introduction

Optical transmission systems advance with higher spectral efficiencies, higher data rates, and simultaneously lower costs [1–12]. In the past decades, wavelength-division and polarization-division multiplexing techniques combined with advanced optical modulation formats have enabled ultra-high spectral efficiencies and data rates. Coherent optical transmission is a key technology for high-capacity long-haul communications with channel data rates at 100 Gb/s and beyond [3, 13–20]. Polarization-division-multiplexed 16-quadrature amplitude modulation (16-QAM) has been utilized in the current 200/400-Gb/s networks [19, 21, 22].

To lower the cost, footprint, and power consumption, the silicon-on-insulator platform is promising for integrated coherent transceivers because of its high refractive index contrast and compatibility with germanium epitaxy growth and implantation. Conventionally, a dual-polarization coherent receiver consists of a number of optical components, such as high-speed photodetectors (PDs) [23], edge couplers [24], polarization splitters and rotators (PSRs) [25, 26], and 90° optical hybrids. To further increase the transmission capacity, recent technological approaches include: (1) advanced modulation formats, such as 32-QAM [27–29], 64-QAM [30–32]; (2) large bandwidth photodetectors, e.g., 50-GHz germanium PD (GePD) [33], 67-GHz graphene based-PD [34] and beyond. They are exploited and implemented to demonstrate a high bit rate on a single channel. On the other hand, the wavelength-division-multiplexing (WDM) technology can be utilized to scale the number of channels in addition to the polarization-division-multiplexing (PDM) method. Therefore, multiple micro-ring resonators (MRRs) or an array waveguide grating (AWG) for separating the lights of individual wavelengths from the bus waveguide are essential optical components for the WDM systems [35, 36]. However, for dense wavelength division multiplexing (DWDM) communication systems, a large number of MRRs or a centimeter-level 50-GHz-spacing AWG [37–39] are required, which introduce additional power consumption and hardly improve the integration level and the subsequent co-packaging process. It is noted that if signals on several wavelengths
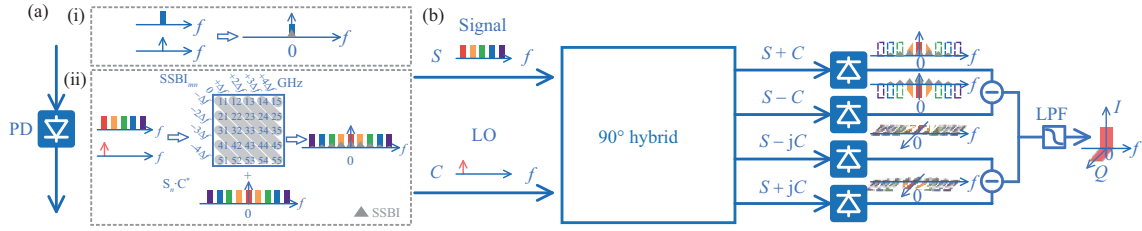

Figure 1 (Color online) (a) Schematic diagram of the beating effect between the LO and WDM signals in an ideal PD. Inset (i) and (ii): the mixing between the LO and signals on single wavelength and five wavelengths, respectively. SSBIs of different frequencies superimpose on the signals of the corresponding frequencies. (b) The hybrid and balanced detection of DWDM signals in our proposed coherent receiver (taking wavelength1 as the CUT). Only signals below about 50 GHz are detected because of the bandwidth limits of GePD, probes, and cables.

are hybridized with the local oscillator (LO) light in a PD, due to the beating effect the photocurrent signals are shifted to their frequency differences from the LO light. Therefore, low-pass filters are required to filter out the photocurrents at high frequencies, and the wavelength of the signal to be demodulated can be switched by changing the wavelength of LO light, thus saving the considerable space required for several micro-ring resonators or AWGs.

In this paper, we present the coherent detection of a 1.12-Tb/s signal using an integrated DWDM and PDM silicon coherent receiver. The proposed coherent receiver achieves coherent detection of DWDM-PDM signal without wavelength demultiplexing devices at the cost of lower received signal power of each hybrid. Low-pass filters are used to filter out the high-frequency noise generated by mixing the LO with signals at different wavelengths from the LO in the photocurrent. The DWDM-PDM signals are split and input into ten 90° hybrids, but only signals of the same wavelength as the LO light can be demodulated and output. This paper is organized as follows. Section 2 describes the principle of the proposed coherent receiver without wavelength division de-multiplexing. Section 3 presents the device design and chip layout. Section 4 demonstrates the detection of five wavelengths of dual-polarization 28-GBaud coherent signals using a silicon receiver. Section 5 gives a conclusion and discussion on the coherent optical transceiver.

2 Principle of the proposed coherent receiver without wavelength de-MUX

In a conventional single-wavelength optical coherent communication system, four hybridized beams of LO (C) and signal (S) lights are injected into each PD. As illustrated in Figure 1(a)(i), the signal-signal beat interference (SSBI) generated by the mixing between themself is superposed on the photocurrents of the baseband signals. However, the SSBI noises and amplified spontaneous emission (ASE) noise can be eliminated by the balanced detection shown as

$$I_1 = \left| \frac{1}{\sqrt{2}} \left(S + C\right) \right|^2 = \frac{1}{2} \left(|S|^2 + |C|^2 + 2\text{Re}\left(S \cdot C^*\right) \right), \tag{1}$$

$$I_2 = \left| \frac{1}{\sqrt{2}} \left(S - C\right) \right|^2 = \frac{1}{2} \left(|S|^2 + |C|^2 - 2\text{Re}\left(S \cdot C^*\right) \right), \tag{2}$$

$$|S|^2 = |S_t|^2 + |n_o|^2 + 2\text{Re}\left(S_t \cdot n_o^*\right), \tag{3}$$

$$I = I_1 - I_2, \tag{4}$$

where S and C represent the signal and LO light, respectively. S_t is the original signal light without ASE noise, namely n_o.

In the case of WDM coherent receivers, a wavelength demultiplexing device is necessary. A typical AWG based on the SOI platform for a DWDM system occupies a footprint of 0.8 cm × 0.8 cm [39], which is several times the size of a single-wavelength PDM coherent receiver. As illustrated in Figure 1(b), when there is no AWG or MRR for wavelength demultiplexing, the LO light (C, taking λ_1 as the channel-under-test (CUT)) and the signals on five wavelengths (S_n, $\lambda_1–\lambda_5$) are mixed in the PD. The obtained photocurrent of the baseband signal is interfered with the SSBI terms generated from the beating between all five tones. The central frequencies of these SSBI noises are determined by the frequency differences

between S_m and S_n. As the input signal light is wavelength division multiplexed, Eqs. (1) and (2) can be rewritten as

$$
\begin{aligned}
I_1 &= \frac{1}{2} \left| C + \sum_{n=1}^{5} (S_n) \right|^2 \\
&= \frac{1}{2} \left(|C|^2 + \sum_{m=1}^{5} \sum_{n=1}^{5} S_m \cdot S_n^* + 2 \sum_{n=1}^{5} \mathrm{Re}\,(S_n \cdot C^*) \right),
\end{aligned}
\tag{5}
$$

$$
I_2 = \frac{1}{2} \left(|C|^2 + \sum_{m=1}^{5} \sum_{n=1}^{5} S_m \cdot S_n^* - 2 \sum_{n=1}^{5} \mathrm{Re}\,(S_n \cdot C^*) \right),
\tag{6}
$$

where m and n represent different wavelengths. Note that S_m $(m = 1, 2, \ldots, 5)$ are on different wavelengths. The second terms of (5) and (6) indicate that when n different signal channels are input into the S port, n^2 spurious responses due to self-mixing (SSBI) will be generated, based on the frequency differences between the channels. For example, if signals on five channels with a frequency spacing of 50 GHz and a LO are the inputs, 1, 2, 3, 4, 5, 4, 3, 2, and 1 SSBIs are superposed on frequencies of $-200, -150, -100, -50, 0, +50, +100, +150,$ and $+200$ GHz, respectively, as depicted in Figure 1(a)(ii). Similarly, the two types of noise ($|S|^2$ and n_o) mentioned above can be suppressed by balanced detection:

$$
\begin{aligned}
I &= I_1 - I_2 = \sum_{n=1}^{5} \mathrm{Re}\,(S_n \cdot C^*), \\
Q &= Q_1 - Q_2 = \sum_{n=1}^{5} \mathrm{Im}\,(S_n \cdot C^*).
\end{aligned}
\tag{7}
$$

According to (7), only the signal with the same wavelength as LO can be demodulated, and signals on the other wavelengths are shifted to the high-frequency region and can be filtered out since the PD normally has a roll-off characteristic. The dashed boxes in Figure 1(b) indicate that the photocurrents above 100 GHz are filtered by PDs (BW$_{3\ \mathrm{dB}} \approx 35$ GHz), while the photocurrents at 50 GHz are partially attenuated. Additional low-pass filters are required to filter out the crosstalk from photocurrent signals around 50 GHz. Therefore, the desired photocurrent signal after the mixing of the signal light and LO is down-converted to the baseband with the frequency spacing of DWDM. Normally there is also a small frequency offset between the desired signal and LO, which could be estimated and eliminated in the electrical domain by advanced DSP.

3 Structural design and fabrication

The silicon coherent receiver integrates the required silicon components for routing and interconnecting photonics elements such as GePDs, edge couplers (ECs), and PSRs. Figures 2(a) and (b) show the block diagram and the microscope photographs of the fabricated receiver, respectively. The receiver comprises six edge couplers, six PSRs, ten 4×4 MMIs, and forty GePDs. The overall footprint of the proposed coherent receiver is 3.87 mm $\times$ 2.8 mm. The chip was fabricated on an SOI wafer with a 220-nm top silicon layer in the Advanced Micro Foundry (AMF, Singapore). The performances of the devices used on the chip were tested at a wavelength of 1550 nm, with the following results. edge coupler: IL $\leqslant$ 2.3 dB/port, 1×2 MMI: IL $\leqslant$ 0.15 dB, Imbalance $\leqslant$ 0.06 dB, PSR: IL$_{\max}$ $\leqslant$ 0.25 dB, PER $\leqslant$ 18.5 dB, 4×4 MMI: IL $\leqslant$ 0.56 dB, Phase error $\leqslant 5°$, GePD: BW$_{3\ \mathrm{dB@3\ V}}$ $\geqslant$ 30 GHz, Responsivity $\geqslant$ 0.7 A/W.

The optical signal containing five wavelengths (λ_1–λ_5) each with two polarizations, is coupled into the signal port of the receiver, while five optical LO lights are coupled into the silicon chip through the other ports. The wavelengths of five input LOs can be out of order since the wavelengths of signal demodulated in each 90° hybrid are selected by the wavelengths of the input LOs. The polarization-multiplexed signal and 45°-polarized LO light, which can be decomposed into x- and y-polarization, are divided and converted into transverse electric (TE) polarizations through six PSRs (one for signal, five for LO). Two TE-polarized signal lights converted from different polarizations are respectively divided into five beams by a 1×2 MMI array and then input to ten 4×4 MMI-based 90° hybrids, whose four optical outputs are detected by four GePDs (see Figure 2(c)). We used a 1×2 MMI array instead of a
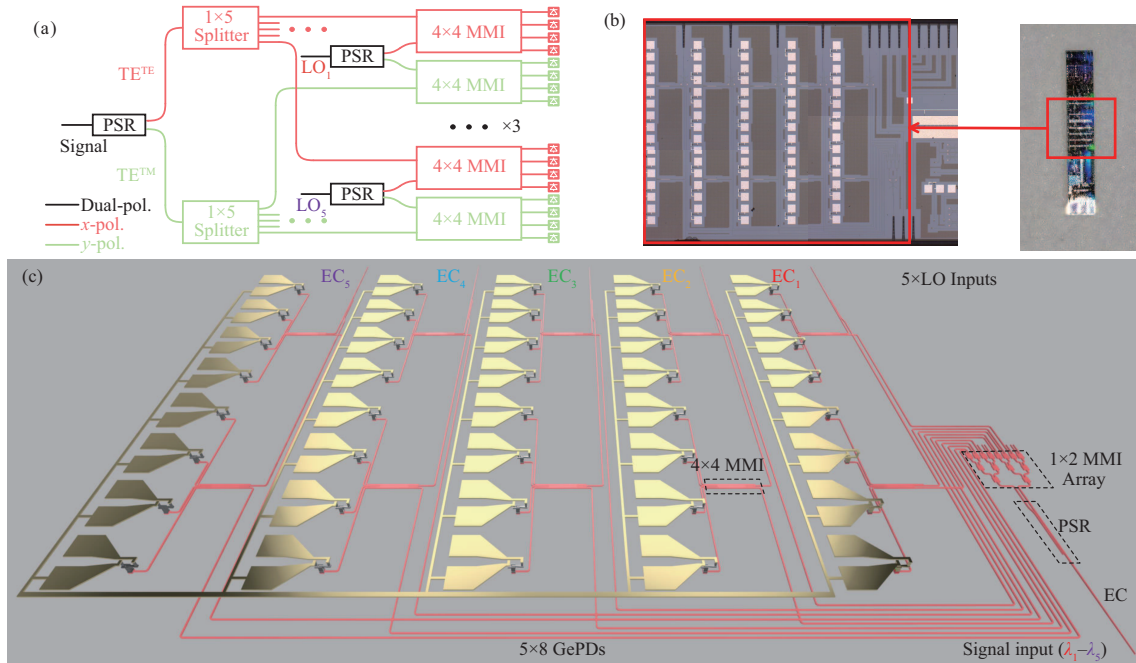
Figure 2 (Color online) (a) Block diagram, (b) microscope photographs, and (c) 3D schematic of the coherent receiver using five wavelengths, two polarizations, EC (edge coupler), PSR, MMI (multi-mode interferometer), and GePD.

1×5 MMI because the former has smaller dimensions, which is more advantageous in reducing the size of the chip. The photocurrents from the four GePDs generate the in-phase and quadrature components of one channel. In general, balanced PDs (BPDs) are required to differentiate the photocurrent signals (I_1 and I_2, Q_1 and Q_2). However, the frequency responses of the integrated GePDs normally have slight differences, which result in receiver-side IQ imbalance and hamper the recovered signal quality. Therefore, in our design, we employ two separate PDs to detect the optical signals and then perform the subtraction operation in digital signal processing (DSP). In a future iteration, we will consider investigating better design to address the non-uniformity issue and employ the balanced photodetector configuration.

4 Experimental setup and results

Figure 3 shows a back-to-back experimental setup to demonstrate the proposed coherent receiver. The experimental demonstration is performed by sending five 224-Gb/s PDM 16-ary quadrature amplitude modulation (16-QAM) signals with different wavelengths into the designed coherent receiver. At the transmitter side, a continuous-wave (CW) light from a tunable laser source (TLS) (SOUTHERN PHOTONICS TLS150, ∼100 kHz linewidth with an output power of 10 dBm) is boosted to 18 dBm using an erbium-doped fiber amplifier (EDFA) and then launched into a commercial in-phase and quadrature modulator (IQM) [6]. The IQM is driven by a 28-GBaud Nyquist 16-QAM signal from a 100 GSa/s digital-to-analog converter (DAC) (MICRAM DAC10002).

Owing to the limited number of CW lasers, we use a wave shaper on another branch to spectrally shape an ASE source [40, 41]. The spectrally shaped signal is combined with the modulated signal by a 50:50 polarization-maintaining coupler to emulate the $4 (= 5 - 1)$ DWDM channels with 50-GHz spacing. Then, the DWDM signal is split into two copies. A fiber delay line is used to decorrelate the two copies. After that, a polarization beam combiner (PBC) is used to combine the two decorrelated copies to generate a PDM signal. Figure 4 shows the optical spectrum after DWDM and PDM.

At the receiver side, the generated 5-DWDM PDM signal is amplified by the EDFA$_3$ before being launched into the fabricated coherent receiver. A tunable OBPF (EXFO XTM-50) is used to filter out the ASE noise and simultaneously select the signals located at the CUT. Since we only have one four-channel digital storage oscilloscope (DSO) (LeCroy 36Zi-A) and one four-channel RF probe array (BW$_{3\,dB}$ > 40 GHz), we can only receive a single-polarization signal at a moment. We use two polarization controllers (PC$_3$ and PC$_4$) to align the polarization states between the optical 16-QAM signal and the LO. For
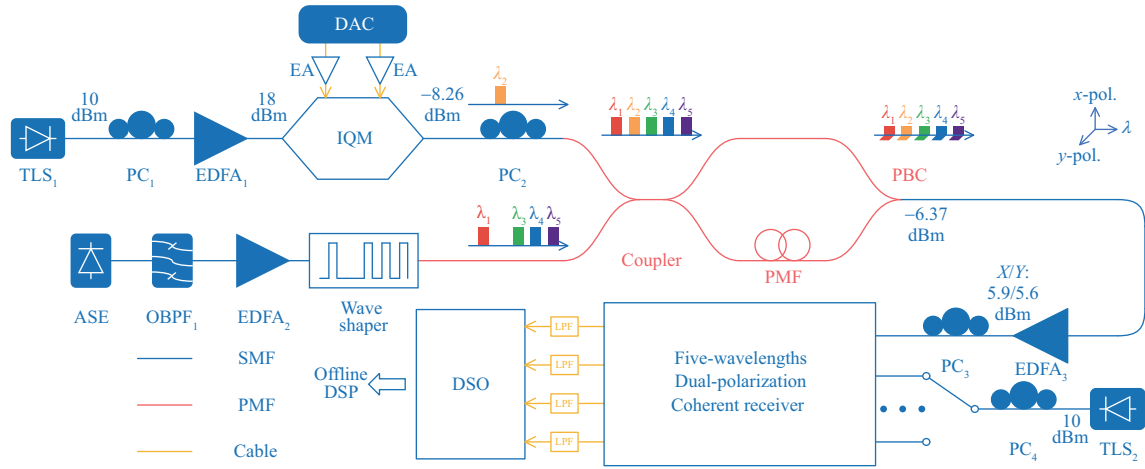
Figure 3 (Color online) Schematic of the experimental setup for generation and detection of the coherent communication system performance of 1.12 Tb/s DWDM-PDM-16QAM from Si PICs. TLS: tunable laser source, PC: polarization controller, EDFA: erbium-doped fiber amplifier, IQM: in-phase and quadrature modulator, DAC: digital-to-analog converter, PBC: polarization beam combiner, DSO: digital storage oscilloscope, SMF: single-mode fiber, PMF: polarization maintaining fiber.
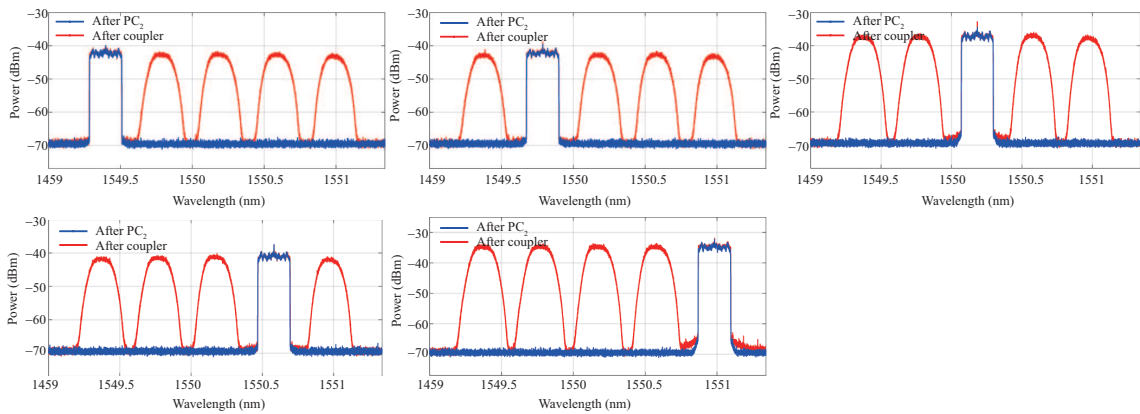

Figure 4 (Color online) The optical spectra of the generated signals of different CUTs, the lights on other wavelengths are ASE noise. The spectra of the two polarizations are identical.
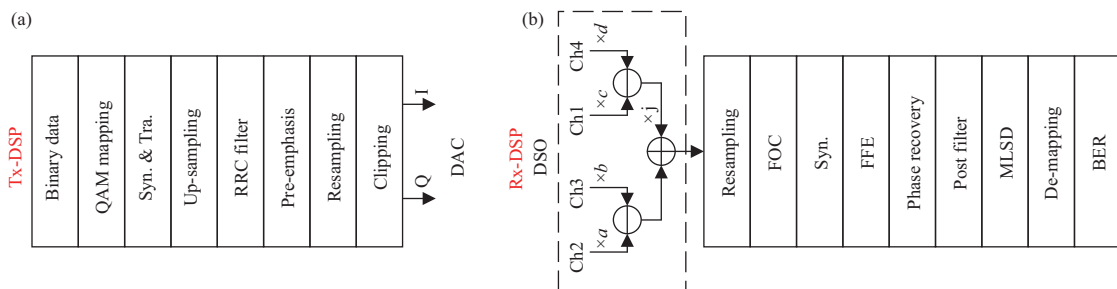

Figure 5 (Color online) DSP algorithms in the (a) transmitter and (b) receiver, respectively.

convenience, we input the x-polarized LO light. Owing to the presence of the PSR, this method is equivalent to inputting 45°-polarized light with twice the intensity. The wavelength of the LO is coarsely aligned with that of the CUT. To achieve larger output powers from the 90° hybrids, the optical power of LO is set to 10 dBm. Four Bias-Tees supply the −2-V bias voltages for the four on-chip GePDs. The received optical signals are converted to electrical signals by optical to electrical (O/E) conversion and then filtered to remove the high-frequency components to avoid spectral aliasing. Finally, the obtained electrical is captured by an 80-GSa/s DSO. Finally, the obtained signals are processed by offline DSP.

Figure 5 presents the utilized DSP algorithms at the transmitter and receiver. At the transmitter, the binary data is mapped to 16-QAM symbols, the synchronization and training sequences are added
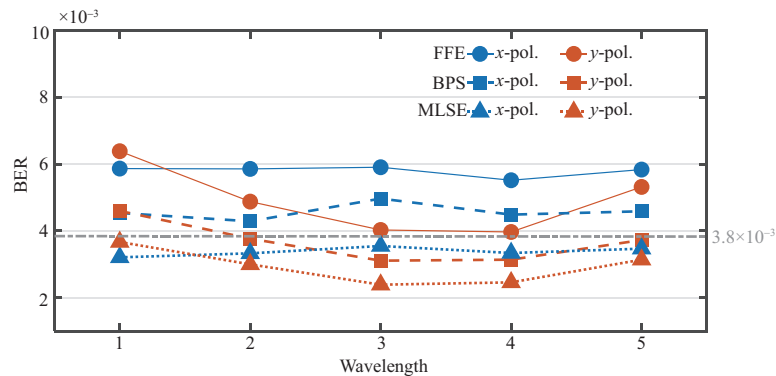
Figure 6 (Color online) The calculated BERs of 28-GBaud 16-QAM signals for ten channels.

at the head of the payload, and the signal pulse is shaped by a root-raised cosine (RRC) filter with a roll-off factor of 0.01. Pre-emphasis is implemented to compensate for the imperfect frequency response of the transmitter-side components. After being resampled to 100 GSa/s, the signals are clipped to suppress the peak-to-power ratio for fully utilizing the dynamic range of the DAC. On the receiver side, the function of BPD is achieved in DSP. Since the responsivities (R) of the fabricated GePDs are not identical, we measure the average amplitudes of the four photocurrents and multiply them by four factors (a, b, c, and d) to keep them balanced. After frequency offset compensation (FOC) and synchronization, the feedforward equalizer (FFE) is utilized to mitigate inter-symbol interference (ISI). The carrier phase recovery is realized by using a blind phase search (BPS) algorithm. Then, we use a post filter to minimize the influence of the noise enhancement effect of the FFE and the maximum likelihood sequence detection (MLSD) is employed for symbol recovery. After de-mapping, the bit error ratio (BER) is calculated.

After obtaining the signal of x-polarisation for wavelength λ_1, we move the radio frequency (RF) probe array to the pads corresponding to the y-polarisation and align the polarization state of LO to y-polarization to sample the y-polarized signal. We then switch the wavelengths of the output lights from two TSLs to λ_2, change the waveshaper setting to suppress the light on the next wavelength λ_2, and repeat the dual polarization data sampling process. After ten rounds of data acquisition, we obtain the data of the ten channels of the 5-DWDM PDM 16-QAM optical communication system.

For the x- and y-polarization, the output powers of the EDFA$_3$, as shown in Figure 3, are 5.9 and 5.6 dBm, respectively. The BERs of ten channels are calculated by error counting and shown in Figure 6. After maximum likelihood estimation (MLSE), the BERs of all ten channels are below the 7% hard-decision forward error correction (HD-FEC) threshold of 3.8×10^{-3}. The BERs of the x-polarization channels are slightly better than that of the y-polarization channels because the insertion loss of the fabricated PSR for the TE mode is smaller than that of the transverse magnetic (TM) mode, and the TE-mode signals propagate through fewer silicon waveguide crossings in the receiver. Figure 7 provides ten constellation diagrams of the recovered DWDM-PDM 16-QAM signals. Thus, we achieve a nominal aggregate net data rate of 1.016-Tb/s (28 GBaud $\times$ 4 bit per symbol $\times$ five wavelengths $\times$ 2 polarizations $\times$ 0.971 (frame redundancy) / 1.07 (7% FEC overhead) = 1.016 Tb/s).

Table 1 compares the chip performance of our scheme with several other receivers using AWG [42–45]. Since the channel spacings are different and the size of AWG is inversely proportional to the channel spacing [46], we have to consider the channel spacing of WDM for fairness. It can be seen that our proposed coherent receiver can establish more channels within the same size and wavelength range, resulting in a higher total communication capacity.

5 Conclusions and discussion

In conclusion, we have proposed and demonstrated a 1.12-Tb/s silicon-integrated coherent receiver for DWDM and PDM transmission. In the proposed receiver, the signal light on two polarizations and five wavelengths is divided by a PSR and a 1×2 MMI array into ten beams, and they are hybridized with the corresponding LO light in different 4×4 MMIs, respectively. As the light is mixed with the LO on the same wavelength, the signals of other wavelengths are shifted to high frequencies due to the beating effect and can be filtered out using an electrical low-pass filter. Compared with the conventional DWDM
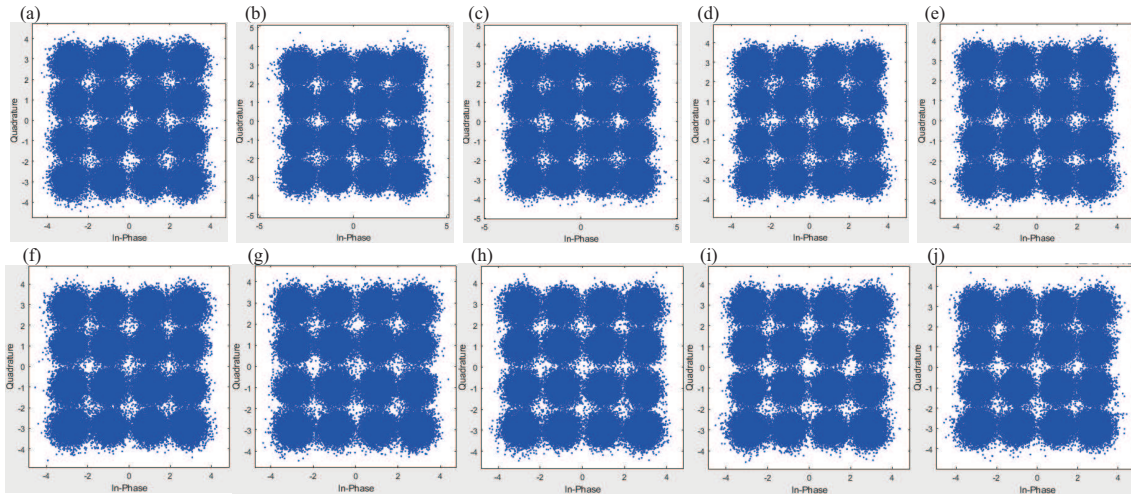
Figure 7 (Color online) Recovered DWDM-PDM 16-QAM (a–e) x- and (f–j) y-constellations at the 50-GHz (0.4-nm) wavelength spacing with ASE noise.

Table 1 Performance of various silicon WDM receiver

Ref.	Material of chip/AWG	Size (mm^2)	Number of channels	Channel spacing (GHz)	Footprint×spacing/channel (mm^2×GHz/channel)
[42]	InP	19.8	4	185	916
[43]	InP/Silica	>469	8	25	>1465
[44], not coherent	Silica	<126	4	800	<25200
[45], not coherent	silicon/SiN	32.5	40	200	162.5
This work	Silicon	10.8	5	50	108

coherent receiver, a large footprint of MRRs or AWG is eliminated, reducing the average footprint and spectrum to about 108 mm$^2 \cdot$ GHz/channel. In the experiment, the 1.12-Tb/s 16-QAM 28-GBaud signals on five wavelengths and two polarizations are successfully recovered, with all BERs below the 7% HD-FEC threshold of 3.8×10^{-3}. This solution saves a large amount of chip area at the cost of degraded signal-to-noise ratio, requiring 6.9 dB higher signal optical power to achieve the same SNR. It is suitable for high-capacity short-range optical communication systems with high integration-level requirements. The footprint required for a DWDM-PDM coherent receiver can be further reduced by a more compact layout or by reducing the sizes of the metal pads to improve the integration of the coherent receiver chip. This approach is scalable to higher rates, e.g., 2 Tb/s or higher, by increasing the baud rate and the number of channels.

References

1 Chralyvy A. The coming capacity crunch. In: Proceedings of European Conference and Exhibition on Optical Communication, 2009

2 Tkach R W. Scaling optical communications for the next decade and beyond. Bell Labs Tech J, 2010, 14: 3–9

3 Ellis A D, Gunning F C G, Cuenot B, et al. Towards 1TbE using coherent WDM. In: Proceedings of Joint Conference of the Opto-Electronics and Communications Conference and the Australian Conference on Optical Fibre Technology, 2008. 1–4

4 Doerr C R, Buhl L L, Baeyens Y, et al. Packaged monolithic silicon 112-Gb/s coherent receiver. IEEE Photon Technol Lett, 2011, 23: 762–764

5 Xia Y, Valenzuela L, Maharry A, et al. A fully integrated O-band coherent optical receiver operating up to 80 Gb/s. In: Proceedings of IEEE Photonics Conference (IPC), 2021. 1–2

6 An S, Zhu Q, Li J, et al. 112-Gb/s SSB 16-QAM signal transmission over 120-km SMF with direct detection using a MIMO-ANN nonlinear equalizer. Opt Express, 2019, 27: 12794–12805

7 Nasu Y, Mizuno T, Kasahara R, et al. Temperature insensitive and ultra wideband silica-based dual polarization optical hybrid for coherent receiver with highly symmetrical interferometer design. Opt Express, 2011, 19: 112–118

8 Tsukamoto S, Ly-Gagnon D S, Katoh K, et al. Coherent demodulation of 40-Gbit/s polarization-multiplexed QPSK signals with 16-GHz spacing after 200-km transmission. In: Proceedings of Optical Fiber Communication Conference, 2005

9 Verbist J, Zhang J, Moeneclaey B, et al. A 40-GBd QPSK/16-QAM integrated silicon coherent receiver. IEEE Photon Technol Lett, 2016, 28: 2070–2073

10 Seiler P M, Voigt K, Peczek A, et al. Multiband silicon photonic ePIC coherent receiver for 64 GBd QPSK. J Lightwave Technol, 2022, 40: 3331–3337

11 Soma G, Ishimura S, Tanomura R, et al. Integrated dual-polarization coherent receiver without a polarization splitter-rotator. Opt Express, 2021, 29: 1711–1721

12 Yamanaka S, Ikuma Y, Itoh T, et al. Silicon photonics coherent optical subassembly with EO and OE bandwidths of over 50 GHz. In: Proceedings of Optical Fiber Communication Conference, 2020

13 Kurata Y, Nasu Y, Tamura M, et al. Silica-based PLC with heterogeneously-integrated PDs for one-chip DP-QPSK receiver. Opt Express, 2012, 20: 264–269

14 Winzer P J, Essiambre R J. Advanced optical modulation formats. In: Optical Fiber Telecommunications VB. Pittsburgh: Academic Press, 2008. 23–93

15 Kikuchi K. Digital coherent optical communication systems: fundamentals and future prospects. IEICE Electron Express, 2011, 8: 1642–1662

16 Wang J, Kroh M, Theurer A, et al. Dual-quadrature coherent receiver for 100G Ethernet applications based on polymer planar lightwave circuit. Opt Express, 2011, 19: 166–172

17 Tsunashima S, Nakajima F, Nasu Y, et al. Silica-based, compact and variable-optical-attenuator integrated coherent receiver with stable optoelectronic coupling system. Opt Express, 2012, 20: 27174–27179

18 Ohyama T, Ogawa I, Tanobe H, et al. All-in-one 112-Gb/s DP-QPSK optical receiver front-end module using hybrid integration of silica-based planar lightwave circuit and photodiode arrays. IEEE Photon Technol Lett, 2012, 24: 646–648

19 Dong P, Liu X, Chandrasekhar S, et al. 224-Gb/s PDM-16-QAM modulator and receiver based on silicon photonic integrated circuits. In: Proceedings of Optical Fiber Communication Conference and Exposition and the National Fiber Optic Engineers Conference (OFC/NFOEC), 2013. 1–3

20 Doerr C, Chen L, Vermeulen D, et al. Single-chip silicon photonics 100-Gb/s coherent transceiver. In: Proceedings of Optical Fiber Communication Conference, 2014

21 Chen L, Doerr C, Aroca R, et al. Silicon photonics for 100G-and-beyond coherent transmissions. In: Proceedings of Optical Fiber Communication Conference, 2016

22 Zhu Y, Zhang F, Yang F, et al. Toward single lane 200G optical interconnects with silicon photonic modulator. J Lightwave Technol, 2019, 38: 67–74

23 Kurata Y, Nasu Y, Tamura M, et al. Heterogeneous integration of high-speed InP PDs on silica-based planar lightwave circuit platform. In: Proceedings of the 37th European Conference and Exhibition on Optical Communication, 2011. 1–3

24 He A, Guo X, Wang K, et al. Low loss, large bandwidth fiber-chip edge couplers based on silicon-on-insulator platform. J Lightwave Technol, 2020, 38: 4780–4786

25 Inoue T, Nara K. Ultrasmall PBS-integrated coherent mixer using 1.8%-delta silica-based planar lightwave circuit. In: Proceedings of the 36th European Conference and Exhibition on Optical Communication, 2010. 1–3

26 Zhang Y, He Y, Jiang X, et al. Ultra-compact and highly efficient silicon polarization splitter and rotator. APL Photonics, 2016, 1: 091304

27 Zhalehpour S, Guo M, Lin J, et al. System optimization of an all-silicon IQ modulator: achieving 100-Gbaud dual-polarization 32QAM. J Lightwave Technol, 2019, 38: 256–264

28 Zhalehpour S, Lin J, Guo M, et al. All-silicon IQ modulator for 100 GBaud 32QAM transmissions. In: Proceedings of Optical Fiber Communication Conference, 2019

29 Wolf S, Going R, Porto S, et al. 2-Channels × 100 GBd 32QAM transmission over 500 km enabled by InP PICs and sige ASICs. In: Proceedings of the 45th European Conference on Optical Communication (ECOC 2019), 2019. 1–3

30 Ishimura S, Fukui T, Tanomura R, et al. 64-QAM self-coherent transmission using symmetric silicon photonic Stokes-Vector receiver. In: Proceedings of Optical Fiber Communication Conference, 2022

31 Fang D, Zazzi A, Müller J, et al. Optical arbitrary waveform measurement (OAWM) on the silicon photonic platform. In: Proceedings of Optical Fiber Communications Conference and Exhibition (OFC), 2021

32 Sano A, Kobayashi T, Ishihara K, et al. 240-Gb/s polarization-multiplexed 64-QAM modulation and blind detection using PLC-LN hybrid integrated modulator and digital coherent receiver. In: Proceedings of the 35th European Conference on Optical Communication, 2009. 1–2

33 Shi T, Su T I, Zhang N, et al. Silicon photonics platform for 400G data center applications. In: Proceedings of Optical Fiber Communications Conference and Exposition (OFC), 2018

34 Wang Y, Li X, Jiang Z, et al. Ultrahigh-speed graphene-based optical coherent receiver. Nat Commun, 2021, 12: 1–7

35 Paiam M R, MacDonald R I. Design of phased-array wavelength division multiplexers using multimode interference couplers. Appl Opt, 1997, 36: 5097–5108

36 Liu X, Hsieh I W, Chen X, et al. Design and fabrication of an ultra-compact silicon on insulator demultiplexer based on arrayed waveguide gratings. In: Proceedings of Conference on Lasers and Electro-Optics, 2008

37 Tsao S L, Lin Y H. Design and analysis of 64 × 64 arrayed waveguide grating based on Silicon-on-Insulator substrat. In: Proceedings of Pacific Rim Conference on Lasers & Electro-Optics, 2005. 957–958

38 Fernando H N J, Stoll A, Boggio J C, et al. Arrayed waveguide gratings beyond communication: utilization of entire image-plane of output star-coupler for spectroscopy and sensing. In: Proceedings of SPIE, 2012. 8431: 372–380

39 Cheben P, Schmid J H, Delage A, et al. A high-resolution silicon-on-insulator arrayed waveguide grating microspectrometer with sub-micrometer aperture waveguides. Opt Express, 2007, 15: 2299–2306

40 He Y, An S, Li X, et al. Record high-order mode-division-multiplexed transmission on chip using gradient-duty-cycle sub-wavelength gratings. In: Proceedings of Optical Fiber Communication Conference (OFC), 2021

41 Son T, Karsten S, Roman D, et al. Beyond 400 Gb/s direct detection over 80 km for data center interconnect applications. J Lightwave Technol, 2020, 38: 538–545

42 Doerr C, Zhang L, Winzer P. Monolithic InP multi-wavelength coherent receiver. In: Proceedings of Conference on Optical Fiber Communication (OFC/NFOEC), Collocated National Fiber Optic Engineers Conference, 2010. 1–3

43 Kaiser R, Saavedra B, Cincotti G, et al. Integrated all-optical 8-channel OFDM/Nyquist-WDM transmitter and receiver for flexible terabit networks. In: Proceedings of the 17th International Conference on Transparent Optical Networks (ICTON), 2015. 1–4

44 Doi Y, Yoshimatsu T, Nakanishi Y, et al. Receiver integration with arrayed waveguide gratings toward multi-wavelength data-centric communications and computing. Appl Sci, 2020, 10: 8205

45 Chen L, Doerr C R, Buhl L, et al. Monolithically integrated 40-wavelength demultiplexer and photodetector array on silicon. IEEE Photon Technol Lett, 2011, 23: 869–871

46 Okamoto K. Fundamentals of Optical Waveguides. Amsterdam: Elsevier, 2021